Digital Doppler Extraction Demonstration With the Advanced Receiver

S. Hinedi, R. Bevan, and H. Del Castillo
Communications Systems Research Section

P. Kinman and D. Chong
Telecommunications Systems Section

R. Labelle
Radio Frequency and Microwave Subsystems Section

This article describes a digital Doppler extraction demonstration with the Advanced Receiver II (ARX II) tracking Pioneer 10 and Voyager 2. The measured results are compared with those of the Block IV receiver that was operating in parallel with the ARX II. It is shown that the ARX II outperforms the Block IV receiver in terms of Allan variance of the Doppler residuals, the amount of which depends on the scenario of interest.

I. Introduction

The Advanced Receiver (ARX) [1] was modified and upgraded to accommodate higher telemetry rates and to enable digital Doppler extraction. The previous receiver (ARX I) underwent several telemetry demonstrations [2–4] at Goldstone, but was unable to perform Doppler extraction because the sampling clock was not fixed, but was an integer multiple of the symbol rate. This is referred to as "synchronous sampling" (synchronous with respect to the symbol epoch). In the new receiver (ARX II) [5], the sampling clock is fixed and is derived from the Frequency and Timing Subsystem (FTS). Hence, sampling is performed asynchronously with the symbol period and may result in a noninteger number of samples per symbol. However, a fixed time base is present in the system and digital Doppler extraction can be performed.

The architecture of the ARX II is discussed in [5] along with the various signal-processing schemes employed to perform the functions of carrier and subcarrier tracking and symbol synchronization, among others. In this article, only the phase-locked loop is described, as it was used to track the residual component of the received signal from the two spacecraft.

Both analog and digital loop closures can be mechanized with the ARX II and both are depicted in Fig. 1. A software command can switch between both methods of loop closure without losing the carrier lock.

In the analog loop closure, the incoming signal is at 70 MHz with about 17-MHz intermediate frequency (IF) bandwidth. It is mixed with an 80-MHz locked reference

to produce the 10-MHz IF, which is sampled at 40 MHz using an 8-bit analog-to-digital converter (A/D). The downconversion to baseband in-phase and quadrature (I and Q) samples is then accomplished by digital mixing using look-up tables. The baseband signal has about an 8-MHz baseband bandwidth and thus a decimation by two is performed to process the signal at the sufficient 20-MHz processing rate (effective sampling rate). The Q samples are accumulated to reduce the rate to the more appropriate loop update rate (50 Hz–1 kHz) to enable a software implementation of the loop filter $F(z)$. The filter output is used to adjust the frequency of a numerically controlled oscillator (NCO), which nominally operates at 4 MHz. The output of the NCO drives a digital-to-analog converter (DAC), producing a 4-MHz analog sine wave, which is mixed with an 84-MHz fixed reference to produce the 80-MHz locked signal that closes the loop.

The operation of the digital loop closure is similar to that of the analog loop closure, except that the 80-MHz signal is a fixed reference and an NCO (running at 10 MHz) is used to close the loop. In this case, the A/D operates on a signal that is not centered at exactly 10 MHz, but rather shifted according to the instantaneous Doppler.

The ARX II accepts an input signal in the 200–400-MHz range from the IF Distribution Assembly output and downconverts it to the 70-MHz range using an external synthesizer (typically a Marconi), as shown in Fig. 2 for the digital loop closure. A total-power automatic gain control (AGC) circuit operates on the signal to ensure that the resulting 10-MHz IF signal lies within the dynamic range of the A/D.

The residual component of the received signal at the output of the AGC can be modeled as

$$r(t) = \sqrt{2P_c}\sin(\omega_i t + \theta_c) + n(t) \tag{1}$$

where P_c denotes the carrier power, ω_i the IF frequency (70-MHz) in rad/sec, and θ_c the carrier phase in radians. The data modulation is ignored here as only the residual carrier component is of interest. The narrowband noise $n(t)$ can be written as

$$n(t) = \sqrt{2}n_c(t)\cos(\omega_i t + \theta_c) - \sqrt{2}n_s(t)\sin(\omega_i t + \theta_c) \tag{2}$$

where $n_c(t)$ and $n_s(t)$ are statistically independent, stationary, band-limited, white-Gaussian-noise processes with one-sided spectral density N_0 watts/Hz and one-sided bandwidth W Hz (roughly 17 MHz in this case). The 70-MHz IF signal is downconverted to 10 MHz and sampled at 40 MHz. Following I and Q mixing, the samples are accumulated to produce

$$I_{cr}(n) = \sqrt{P_c}\cos\phi_c(n) + n_I(n) \tag{3}$$

$$Q_{cr}(n) = \sqrt{P_c}\sin\phi_c(n) + n_Q(n) \tag{4}$$

where $n_I(n)$ and $n_Q(n)$ are independent Gaussian random variables with variances $N_0/2T_u$, where T_u denotes the loop update period and $\phi_c(n)$ the carrier phase error. The Q_{cr} samples update the loop filter, which is given by

$$F(z) = G_1 + \frac{G_2}{1-z^{-1}} + \frac{G_3}{(1-z^{-1})^2} \tag{5}$$

where

$$G_1 = rd/T_u \tag{6}$$

$$G_2 = rd^2/T_u \tag{7}$$

$$G_3 = krd^3/T_u \tag{8}$$

and

$$d = 4B_L T_u(r-k)/r(r-k+1) \tag{9}$$

where B_L is the design loop bandwidth in hertz, r is typically 2 or 4 and is equal to 4ξ (where ξ is the damping ratio), and k is a type-III loop gain parameter ($k = 0$ for a type-II loop) with typical values ranging from 1/4 to 1/2.

Digital Doppler extraction consists of recording the phase estimate of the incoming waveform time tagged to station time using a Time Code Translator (TCT). The resolution of Doppler data depends heavily on the number of bits used in the NCO to represent phase and frequency.

In the digital loop closure, the NCO accumulates fractional phase using 32 bits, but only the most significant 12 bits are used in the sin/cos look-up table. This results in a phase resolution of 0.24 mcycle (2^{-12}). The phase is recorded, external to the NCO, using 48 bits for the integer part and 12 bits for the fractional part. The NCO, in this case, operates at a nominal frequency of 10 MHz and is clocked by a 40-MHz clock. This results in 9.3-mHz ($4 \times 10^7/2^{32}$) frequency resolution.

In the analog loop closure case, the fractional phase is recorded using 14 bits, two of which are accumulated external to the NCO. The resulting phase resolution is 0.06 mcycle, better than that of the digital loop closure. The NCO,

in this case, is actually operating at a nominal frequency of 16 MHz with a 20-MHz clock, but it effectively produces a 4-MHz signal because of the additional bits. The resulting frequency resolution is 1.16 mHz ($2 \times 10^7/2^{34}$), better than the digital loop case.

However, the improved resolution for the analog loop case is at the expense of limiting the maximum nominal frequency to one-fourth of the clock rate (the practical limit of an NCO is roughly 40 percent of the clock rate). That in turn limits the dynamic excursion of the frequency to ±1 MHz in the analog loop closure, whereas it is about ±5 MHz in the digital closure. Time tagging is performed at ±1 μsec accuracy with a ±1 nsec stability. The logging rate can be chosen by software from 1, 2, 5, 10, or 20 Hz.

II. Demonstration Description and Results

The demonstration consists of operating the ARX II in parallel with the Block IV receiver; both track the same spacecraft. Both receivers record data for an identical period of time. The data are later analyzed to quantify and compare the respective performances (see Fig. 3). In all the results to follow, the ARX II was operating with a 500-Hz loop update rate.

A. Allan Variance

The X-band downlink of Voyager 2 (channel 14, 8415.000000 MHz) and the S-band downlink of Pioneer 10 (channel 7, 2292.407407 MHz) were tracked to determine the relative effectiveness of the ARX II and the Block IV receiver in Doppler measurements.

Doppler residuals from four data arcs, as defined in Table 1, are reported here. The first arc is from the Voyager-2 X-band downlink tracked on Greenwich Day of Year (DOY) 195, the second from the Pioneer-10 downlink tracked on DOY 195, and the last two from the Pioneer-10 downlink tracked on DOY 201. During all of these tracks, the spacecraft operated in a three-way Doppler mode, thus eliminating problems associated with the spacecrafts' onboard oscillators. For each of these arcs, the downlink was simultaneously tracked by the ARX II and a Block IV receiver. The downconverted carrier phase as measured by the ARX II was recorded once per second and the Doppler count as measured by the Block IV Doppler extractor was recorded once per second.

Use was made of two time scales during the analysis: a 24-hour clock for Greenwich Mean Time and the number of seconds past the January 1, 1950 epoch. This "J 50" time was needed to do a linear interpolation on the uplink frequencies as reported in the Program Frequency Records (Table 2).

The Doppler observable is calculated for the ARX II as

$$f_{DO} = 48Gf_E + f_{NCO} - f_1 - f_2 - f_3 \qquad (10)$$

where f_{DO} is the Doppler observable, G the transponder ratio (880/221 for the Voyager track and 240/221 for the Pioneer tracks), f_E the exciter frequency, f_{NCO} the difference in phase as measured one second apart by the ARX II, f_1 the frequency of the first local oscillator (8.1 GHz for the Voyager track, 2.0 GHz for the Pioneer tracks), f_2 the frequency of the second local oscillator, and finally, f_3, which is 80 MHz for digital closure and 74 MHz for analog closure of the ARX II loop.

The exciter operates at approximately 44 MHz, whereas the Program Frequency Records report the exciter frequency divided by two (approximately 22 MHz). The exciter frequency is found by interpolating the frequency ramps of Table 2 and then multiplying by two. The second local oscillator is a Marconi synthesizer; its setting for each of the tracks is given in Table 3. The final term in Eq. (10) depends on whether the ARX II had digital or analog loop closure; this information is given in Table 4.

Prior to DOY 201, there was a hardware clocking problem that caused the cycle count recorded by the ARX II to be low by exactly one cycle on some (randomly occurring) samples and these were processed by a cycle correction algorithm that was used to correct the data. The DOY 201 data did not need to be processed by this algorithm because the hardware problem was fixed by that date.

The Doppler residual is calculated from the Doppler observable as

$$f_\Delta = f_{DO} - f_M - f_T \qquad (11)$$

where f_Δ is the Doppler residual, f_M the modeled (based on trajectory) Doppler observable, and f_T the tropospheric correction.

Equation (11) applies to both the ARX II Doppler residual and to the Block IV Doppler residual. The Block IV Doppler observable, the modeled Doppler observable, and the tropospheric correction are all available on the REGRES file provided by navigation personnel.

Doppler residuals, spaced one second apart, were calculated for both receivers for each of the four data arcs defined in Table 1. The Doppler residual record for part of the Voyager 195 data arc is shown in Fig. 4. In that figure, a bias was added to the Block IV residuals to displace them from the ARX II residuals so that the two traces could be discerned. In fact, the means of those two traces are in excellent agreement. The mean values of the Doppler residuals for the ARX II and for the Block IV receiver are given in Table 5. It is noted that the two receivers agree on the magnitude of the Doppler effect to less than 1 mHz.

The square-root Allan variance is used here to characterize the jitter in the Doppler residual measurements. It is defined as

$$\sigma_y(\tau) = \frac{1}{\sqrt{2}\nu}\sqrt{< [f_\Delta(t+\tau) - f_\Delta(t)]^2 >} \qquad (12)$$

where $\sigma_y(\tau)$ is the square-root Allan variance, τ the integration time, ν the downlink frequency, and $< \cdot >$ denotes the time average over the entire data arc. The square-root Allan variances computed for a one-second integration time are contrasted in Table 6. Also given in Table 6 are modeled values of that quantity based on the assumption that downlink thermal noise dominates the frequency instability for such a short integration time. The modeled values came from [6], i.e.,

$$\sigma_y(\tau) = \frac{1}{2\pi\tau\nu}\sqrt{\frac{3B_L}{P_c/N_0}} \qquad (13)$$

where P_c/N_0 denotes the carrier power-to-noise spectral density ratio (from Table 4) and B_L the one-sided loop bandwidth.

The modeled and measured variances for short integration times as presented in Table 6 agree closely for the Pioneer tracks, indicating that the Doppler measurement error really is dominated by downlink thermal noise. For the Voyager 195 track, the measured variance is somewhat higher than the modeled variance; this could be due to the carrier power not being constant during the pass.

The square-root Allan variance of the Doppler residual is plotted as a function of integration time in Figs. 5 and 6 for Voyager and Pioneer, respectively. These plots show a thermal noise dominance with reciprocal τ dependence for the smaller integration times, and the advantage of the ARX II's smaller loop bandwidth is made plain. For larger integration times, other error sources dominate and the bandwidth advantage of the ARX II is lost. With the Pioneer data, the two traces actually begin to coalesce, indicating a common error source for the two receivers. This common error source, which dominates for larger integration times, is almost certainly solar plasma. The Sun-Earth-probe angle was 38.2 deg for Pioneer on DOY 195. The Pioneer 201 data arcs are not long enough to provide a statistically significant Allan variance for the longer integration times.

B. Receiver Tracking Performance

The ARX II acquires the carrier using an automated procedure, which consists of performing several software fast Fourier transforms (FFTs) around the frequency predict. The size and the rate of the FFTs are controlled by software, and the spectra are noncoherently averaged to reduce the noise. The largest peak is then selected and the loop enabled. The acquisition time depends on the speed of the FFT computation. A future upgrade is planned that will use a dedicated FFT board to perform the computations. This will dramatically reduce the acquisition time to less than a second.

For performance evaluation, the ARX II records several parameters. These include: carrier power-to-noise, spectral, density-level estimates, $\widehat{P_c/N_0}$; averaged and normalized I and Q samples; steady-state phase-error estimates $\widehat{\phi_{ss}}$, etc.

The averaged I sample can be used in real time to monitor the loop gain and, hence, the loop bandwidth. With proper normalization, the averaged I samples should be unity, assuming that the amplitude of the incoming signal is "close" to its predict and, hence, that the operating loop bandwidth is its designed value. That averaging should be performed when the steady-state error due to dynamics is negligible; otherwise, no information about loop gain can be deduced. A steady-state phase-error estimate can be obtained in real time by computing

$$\widehat{\phi_{ss}}(j) = \tan^{-1}\left(\frac{\sum_{n=j}^{n=j+L+1} Q_{cr}(n)}{\sum_{n=j}^{n=j+L+1} I_{cr}(n)}\right) \qquad (14)$$

where L controls the estimation period. In the ARX II, $\widehat{\phi_{ss}}(j)$ can be sent to the monitor's screen at different rates ranging from once every second to once every minute. Another key parameter is the incoming P_C/N_0, which is also estimated by the receiver according to

$$\widehat{\frac{P_c}{N_0}}(j) = \frac{\left(\sum_{n=j}^{n=j+L+1} I_{cr}(n)\right)^2}{2T_u \sum_{n=j}^{n=j+L+1} Q_{cr}^2(n)} \qquad (15)$$

Figure 7 depicts the various parameters for a Pioneer track using analog loop closure with a type-III loop. In this case, the estimation period was 10 sec and the designed loop bandwidth about 0.6 Hz. It is clear that the averaged I is close to unity and the averaged Q close to zero, which indicates that the operating bandwidth is 0.6 Hz, as designed. The estimated P_c/N_0 is roughly 12.5 dB-Hz (compared with a 13 dB-Hz predict) and the steady-state phase error is approximately zero.

In Fig. 8, Pioneer results are also shown for the digital loop closure case with a type-II loop. The averaged Q is no longer zero as expected, due to the 7-deg steady-state phase error (since type-II loops cannot track Doppler rates with zero phase error). The resulting P_c/N_0 estimates are also degraded by about 0.6 dB to yield roughly 11.9 dB-Hz. Finally, Fig. 9 depicts the results for a Voyager 2 track using a type-III loop with digital closure. Note that the normalized I is not unity, which implies that the operating loop bandwidth is actually 2.5 Hz (1.2 times the designed bandwidth of 2 Hz). The steady-state error is zero as expected and the estimated P_c/N_0 is about 31.3 dB-Hz (compared with a 32-dB-Hz predict). The estimation period for the Voyager data is one second due to the relatively "strong" signal.

III. Conclusion

This article described digital Doppler extraction with the ARX II and the results were compared to the Block IV receiver Doppler extractor. It was shown that digital Doppler extraction did not result in any degradation relative to Block IV, and in most cases performed better with the ARX II. From the standpoint of Doppler extraction performance, ARX II is an excellent candidate for future Block V receiver implementation.

Acknowledgments

We would like to thank Joseph Statman, Ernest Stone, and Ted Peng for their encouragement, and Robert Johnson and Miguel Marina for their help as test coordinators. We would like to thank the personnel of DSS 14 and their representatives in the Modified Configuration Control Board for allowing us to be out there at a time when they were busy preparing for the Voyager 2 Neptune encounter. We thank the Pioneer 10 and Voyager 2 Projects for allowing us to tap into their signals. We thank Gene Goltz and Gil Roldan of the Navigation Systems Section for preparing Block IV REGRES files, and Stanley Mak of the TDA Mission Support and DSN Operations Section for preparing predicts. Many others contributed ideas and background information that led to the successful conclusion of these tests; these people are mainly from the following organizations: the Navigation Systems Section, the DSN Data Systems Section, the TDA Engineering Section, and the TDA Mission Support and DSN Operations Section.

References

[1] D. Brown and W. Hurd, "DSN Advanced Receiver: Breadboard Description and Test Results," *TDA Progress Report 42-89,* Jet Propulsion Laboratory, Pasadena, California, pp. 48–66, May 15, 1987.

[2] D. Brown, W. Hurd, V. Vilnrotter, and J. Wiggins, "Advanced Receiver Tracking of Voyager 2 Near Solar Conjunction," *TDA Progress Report 42-93,* Jet Propulsion Laboratory, Pasadena, California, pp. 75–82, May 15, 1988.

[3] W. Hurd, D. Brown, V. Vilnrotter, and J. Wiggins, "Telemetry SNR Improvement Using the DSN Advanced Receiver With Results for Pioneer 10," *TDA Progress Report 42-93,* Jet Propulsion Laboratory, Pasadena, California, pp. 64–74, May 15, 1988.

[4] V. Vilnrotter, W. Hurd, and D. Brown, "Optimized Tracking of RF Carriers With Phase Noise, Including Pioneer 10 Results," *TDA Progress Report 42-91,* Jet Propulsion Laboratory, Pasadena, California, pp. 141–157, November 15, 1987.

[5] S. Hinedi, "Functional Description of the Advanced Receiver," *TDA Progress Report 42-100,* Jet Propulsion Laboratory, Pasadena, California, February 15, 1990.

[6] J. A. Barnes, et al., "Characterization of Frequency Stability," *IEEE Transactions on Instrumentation and Measurement,* vol. IM-20, no. 2, pp. 105–120, May 1971.

Table 1. Definition of tracks

Track	Start time		End time	
	hh:mm:ss	J 50 Time, sec	hh:mm:ss	J 50 Time, sec
Voyager 195	06:41:00	1247553660	07:52:00	1247557920
Pioneer 195	14:11:00	1247580660	14:52:00	1247583120
Pioneer 201A	12:18:00	1248092280	12:35:00	1248093300
Pioneer 201B	14:46:00	1248101160	15:07:00	1248102420

Table 2. Data from Program Frequency Records

Pass	Time, J 50, sec	Start frequency, Hz	Ramp rate, Hz/sec
V195	1247552633	$0.2201533673236050D+08$	$0.2295000000000000D-02$
V195	1247557733	$0.2201534843686050D+08$	$0.2235000000000000D-02$
P195	1247573336	$0.2198478999999950D+08$	$0.0000000000000000D+00$
P201	1248089640	$0.2198462999999950D+08$	$0.0000000000000000D+00$

Table 3. Second local oscillator frequency

Track	Second local oscillator (f_2), Hz
Voyager 195	244416020
Pioneer 195	222078470
Pioneer 201A	222094640
Pioneer 201B	222094640

Table 4. Receiver parameters

Track	P_c/N_0, dB-Hz	Block IV One-sided loop bandwidth, Hz	ARX II One-sided loop bandwidth, Hz	ARX II Loop closure
Voyager 195	30	54	2.0	Digital
Pioneer 195	11	2.5	2.0	Digital
Pioneer 201A	11	2.5	1.0	Digital
Pioneer 201B	11	2.5	0.6	Analog

Table 5. Mean of Doppler residual

Track	Mean of Doppler residual, Hz	
	Block IV	ARX II
Voyager 195	−0.130	−0.130
Pioneer 195	−0.153	−0.153
Pioneer 201A	−0.148	−0.147
Pioneer 201B	−0.149	−0.149

Table 6. Square-root Allan variance of Doppler residuals

Track	1-second (square-root) Allan variance of Doppler residuals			
	Block IV		ARX II	
	Modeled	Measured	Modeled	Measured
Voyager 195	7.6×10^{-12}	1.1×10^{-11}	1.5×10^{-12}	2.3×10^{-12}
Pioneer 195	5.4×10^{-11}	5.1×10^{-11}	4.8×10^{-11}	4.7×10^{-11}
Pioneer 201A	5.4×10^{-11}	5.4×10^{-11}	3.4×10^{-11}	2.9×10^{-11}
Pioneer 201B	5.4×10^{-11}	5.4×10^{-11}	2.6×10^{-11}	1.9×10^{-11}

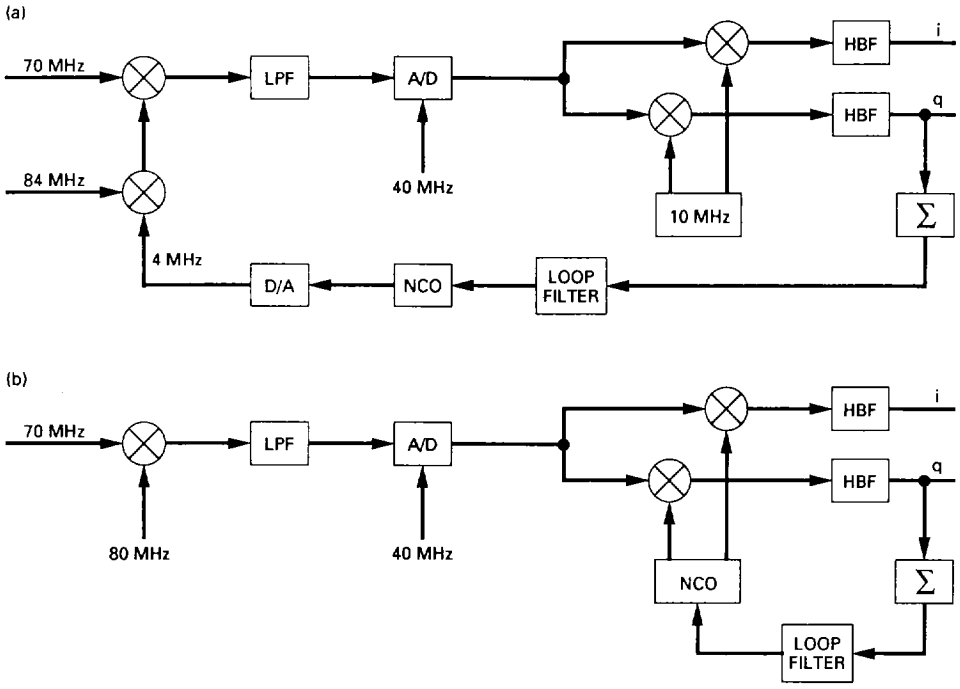

Fig. 1. Analog versus digital loop closure.

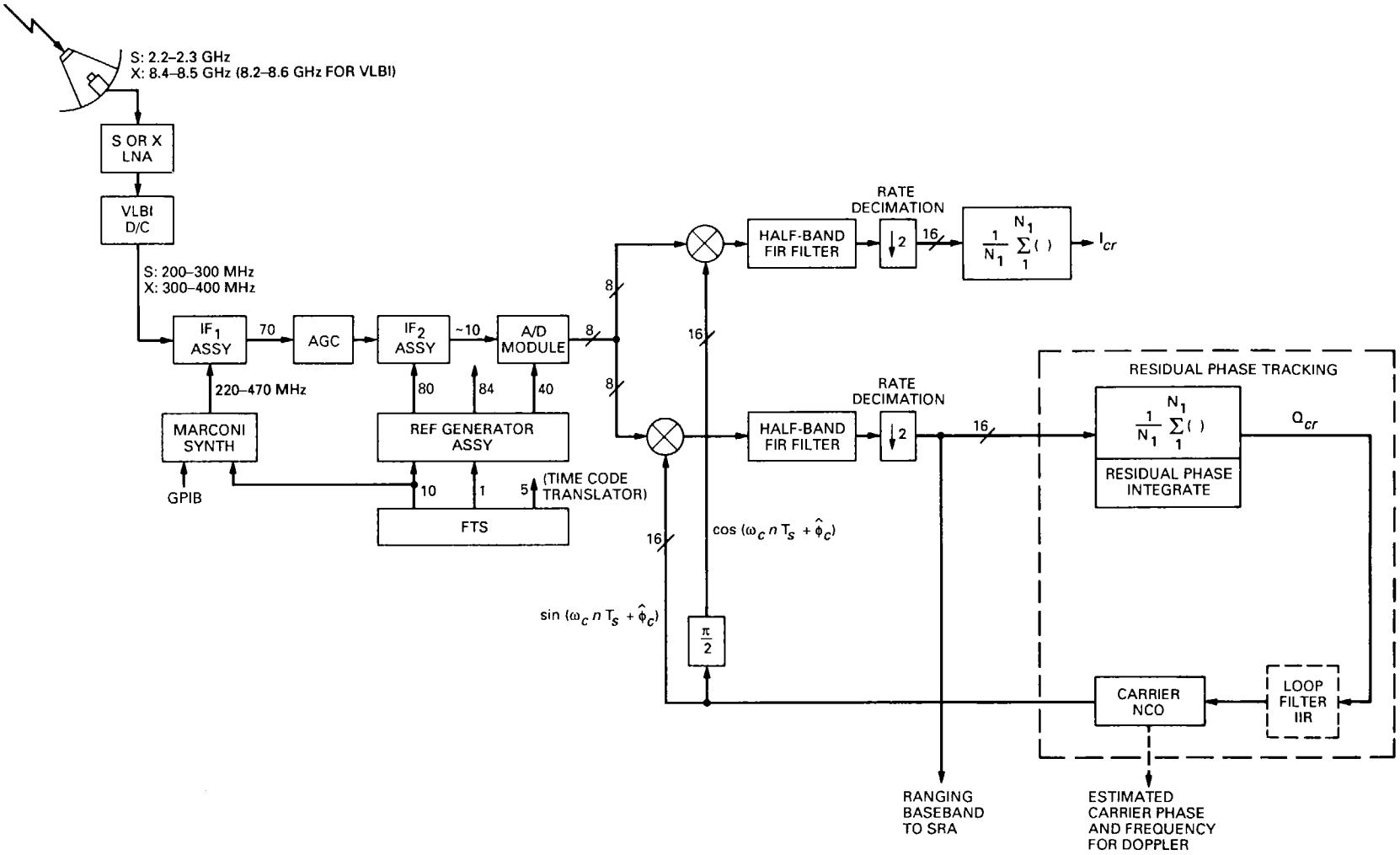

Fig. 2. ARX II phase-locked loop.

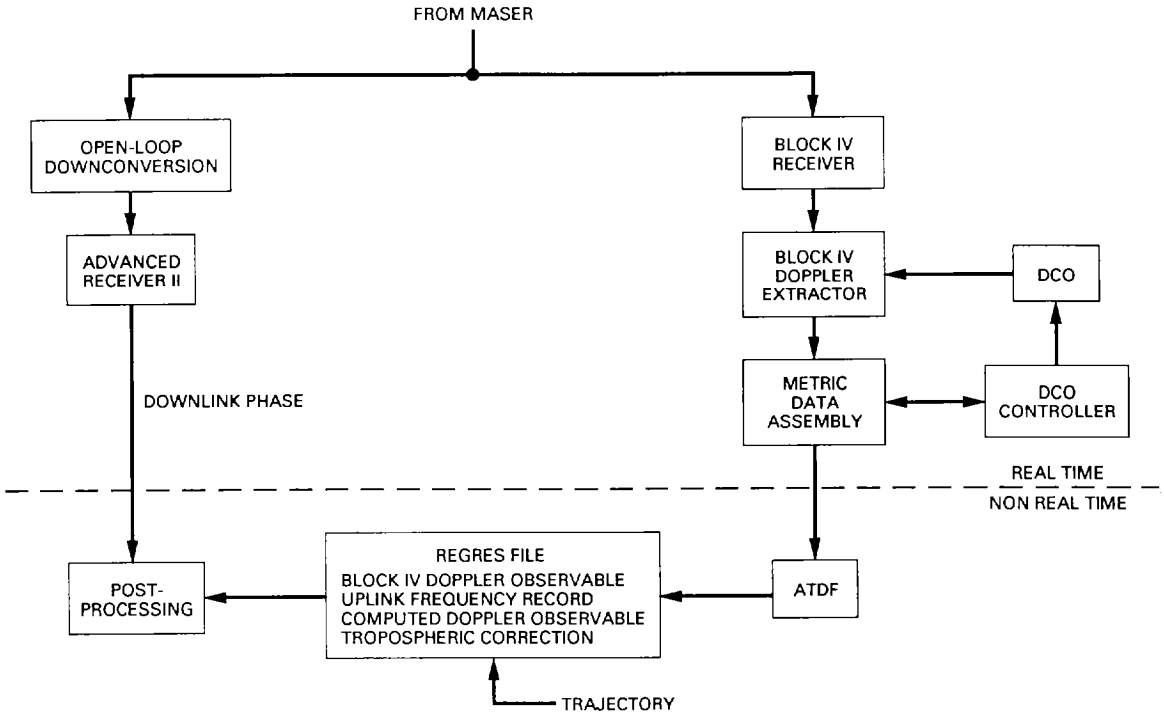

Fig. 3. Experiment description.

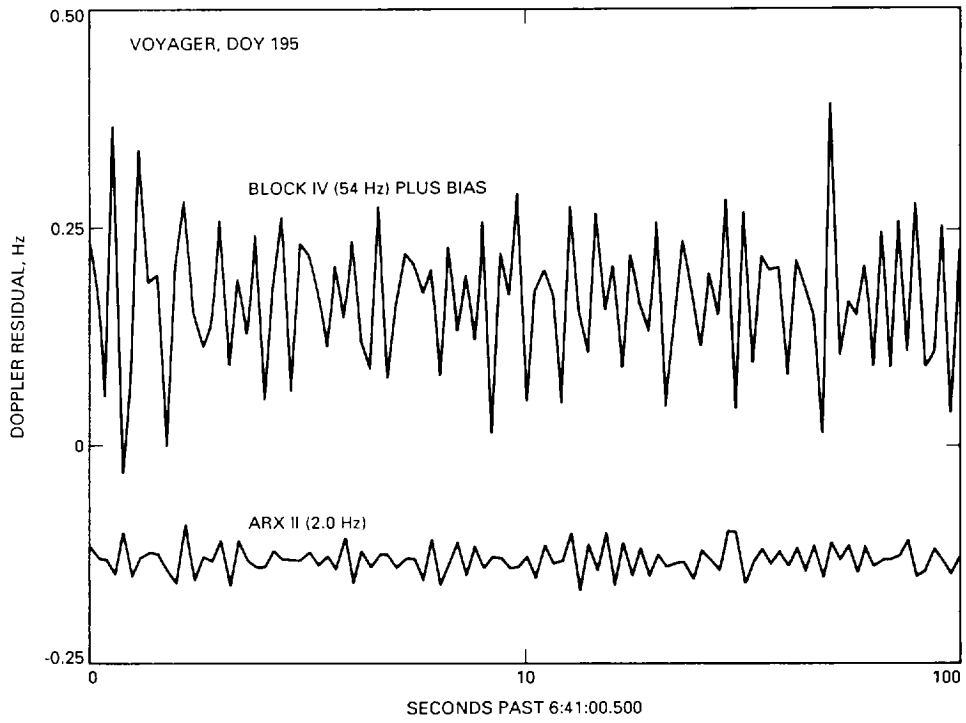

Fig. 4. Doppler residual for Voyager 2, DOY 195.

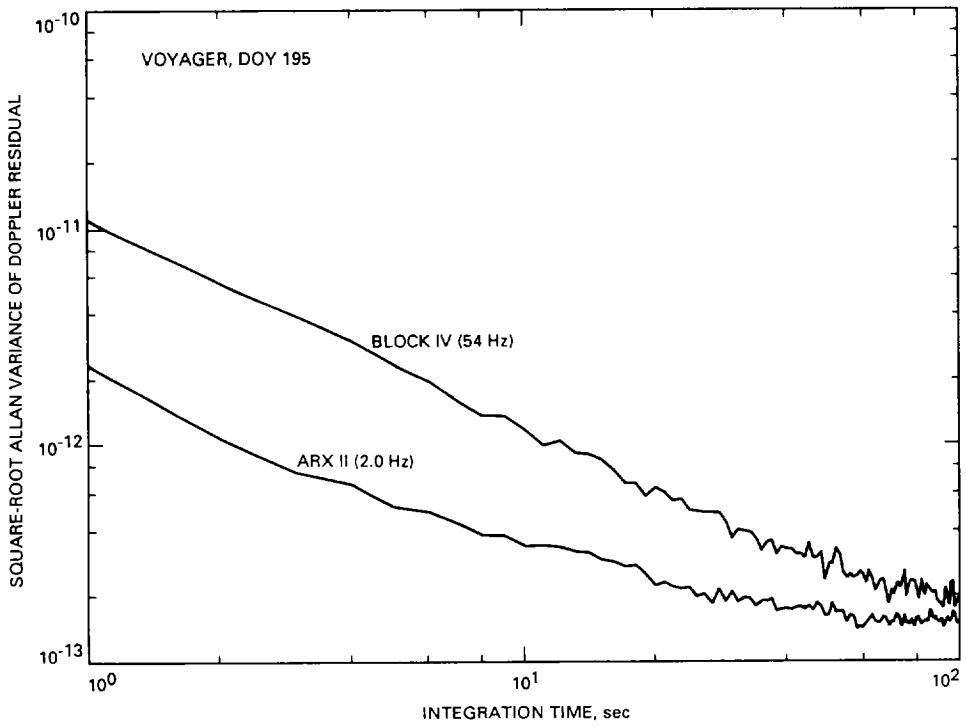

Fig. 5. Allan variance of Doppler residual for Voyager 2, DOY 195.

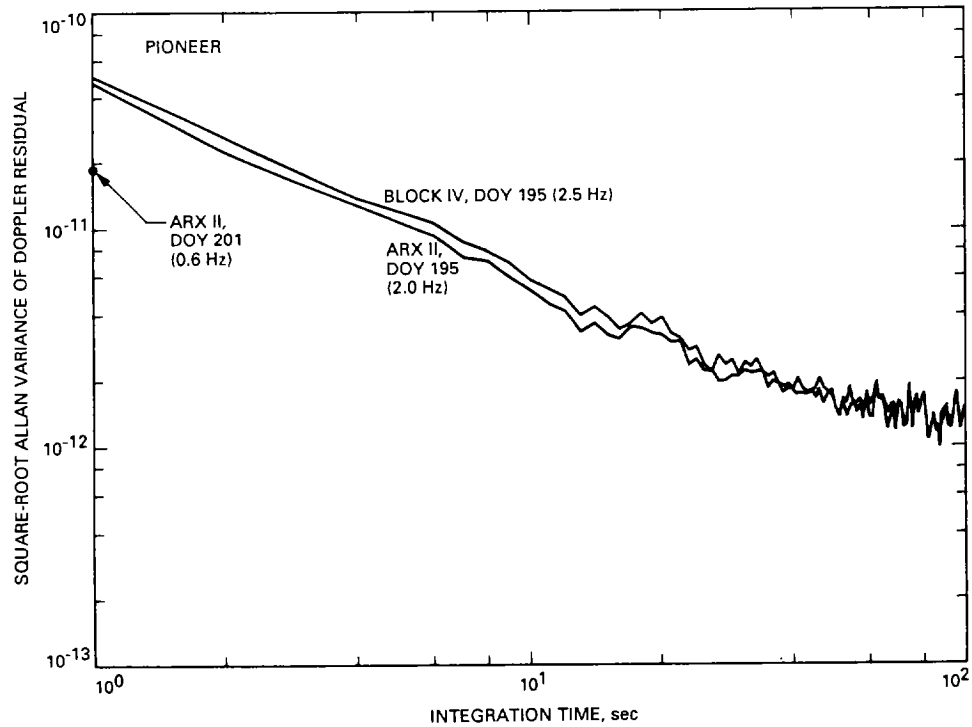

Fig. 6. Allan variance of Doppler residual for Pioneer 10, DOY 195.

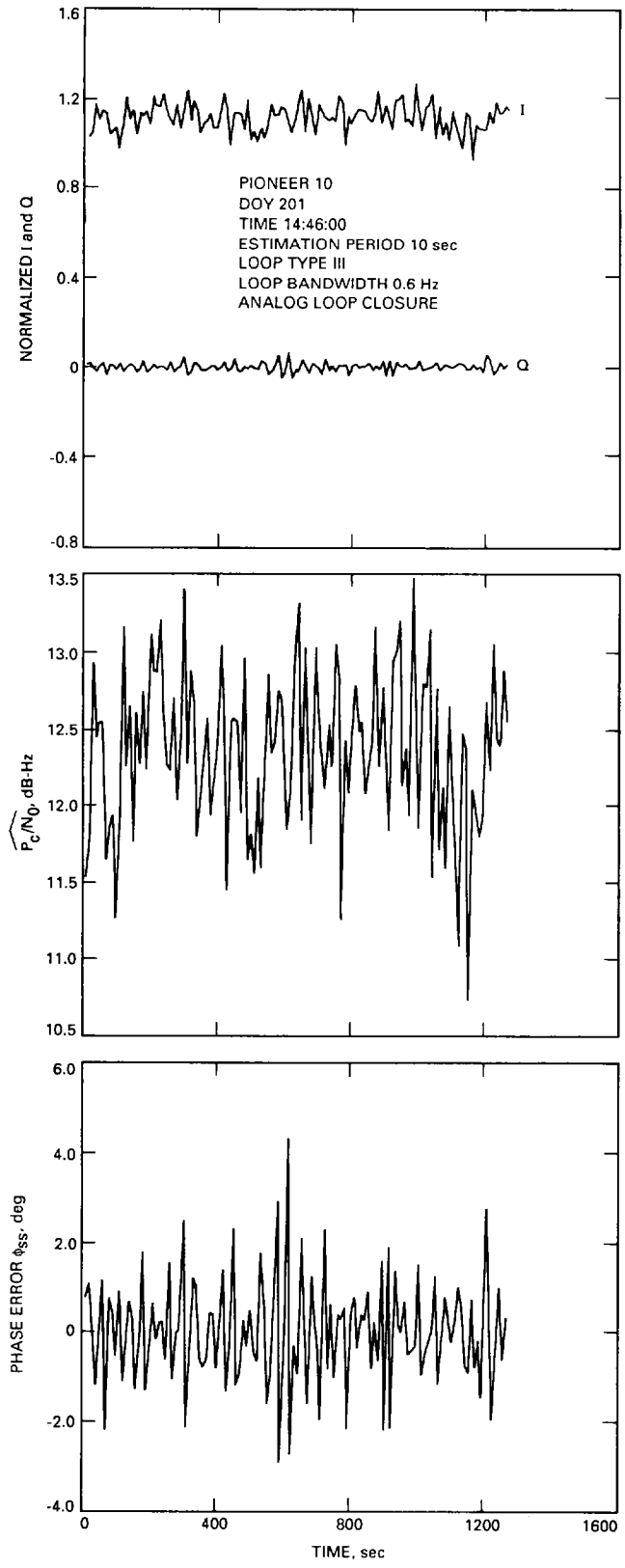

Fig. 7. ARX II data for Pioneer 10, DOY 201.

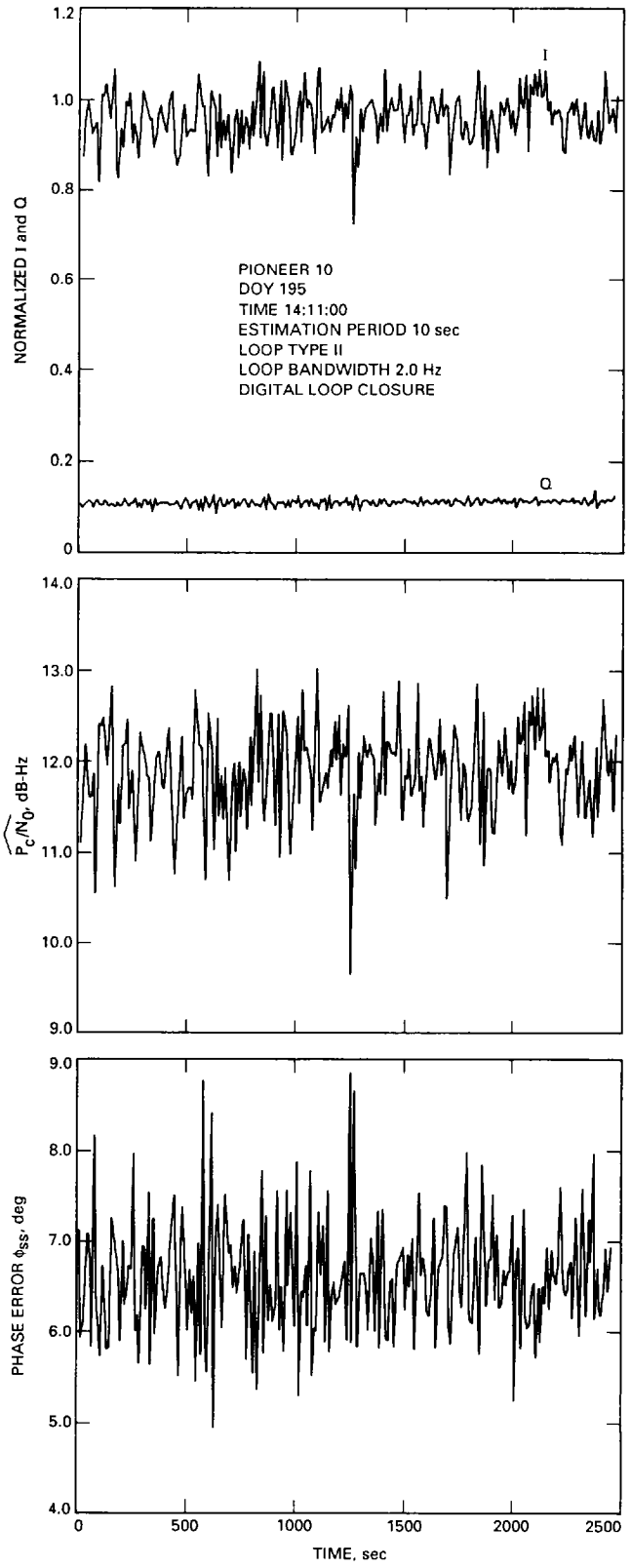

Fig. 8. ARX II data for Pioneer 10, DOY 195.

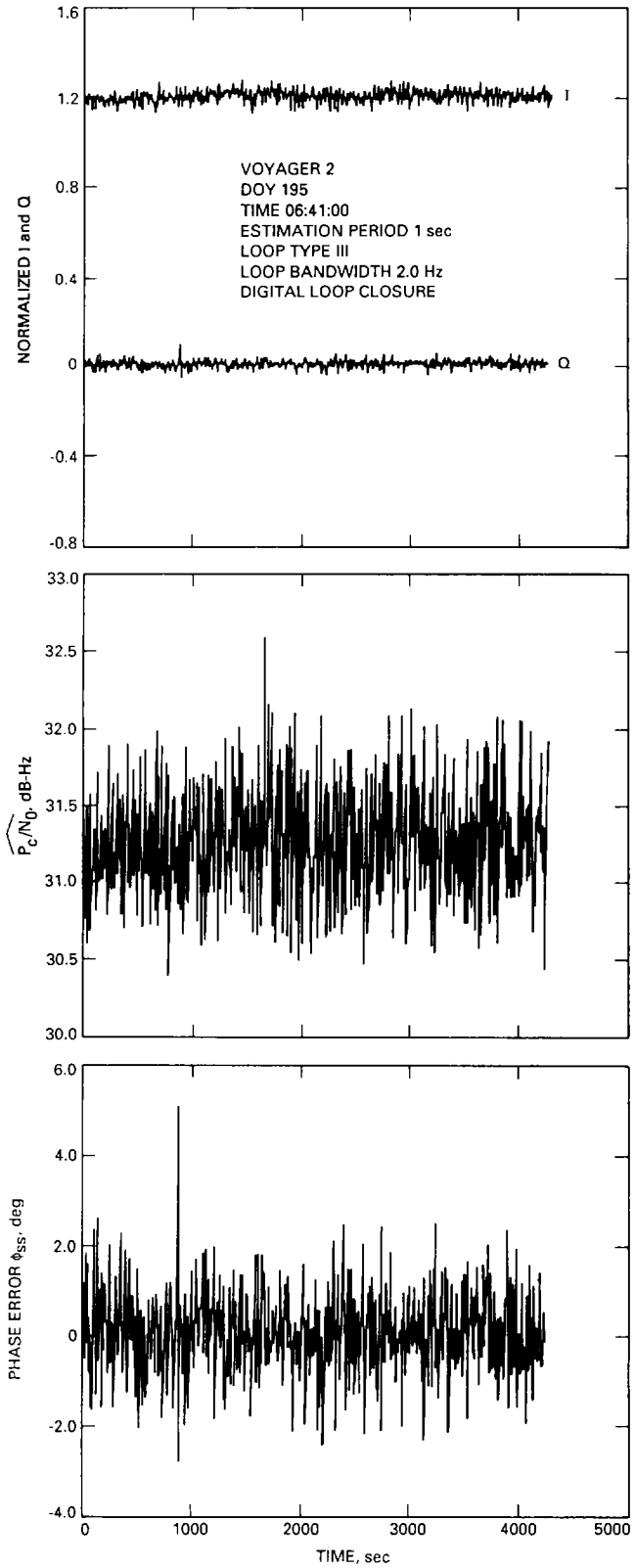

Fig. 9. ARX II data for Voyager 2, DOY 195.